Invariant Interest Point Detection Based on Variations of the Spinor Tensor

Anders Hast
Uppsala University,
Uppsala, Sweden
anders.hast@it.uu.se

Andrea Marchetti
IIT, CNR
Pisa, Italy
andrea.marchetti@iit.cnr.it

ABSTRACT

Image features are obtained by using some kind of interest point detector, which often is based on a symmetric matrix such as the structure tensor or the Hessian matrix. These features need to be invariant to rotation and to some degree also to scaling in order to be useful for feature matching in applications such as image registration. Recently, the spinor tensor has been proposed for edge detection. It was investigated herein how it also can be used for feature matching and it will be proven that some simplifications, leading to variations of the response function based on the tensor, will improve its characteristics. The result is a set of different approaches that will be compared to the well known methods using the Hessian and the structure tensor. Most importantly the invariance when it comes to rotation and scaling will be compared.

Keywords

Interest Point Detector; Features; Invariance; Spinor Tensor; Harris Detector; Hessian matrix.

1 INTRODUCTION

Several novel interest point detectors based on the spinor tensor are proposed and it is shown that they are invariant.

Interest points are used as base points for comparing image features for many types of applications in many fields of computer vision, such as tracking [ST94], image registration and stitching [BL07, Sze06], just to mention a few.

Several methods for extracting such interest or feature points from images have been proposed. Some of the most notable are the Harris corner detector [HS88], which is based on the so called structure tensor and the determinant of the Hessian, used for SURF [BETVG08]. Another approach is based on the difference of Gaussians (DOG), which is used for SIFT [Low04, BL07]. More feature point detectors are found in literature such as [TH98, SB97] and several overviews of different detectors have been published [SMB98, SMB00, TM07, GHT11, ZKM04].

A novel interest point detector is investigated, which is based on the so called spinor tensor. It will be shown that it is invariant to rotation and to some degree to scaling. Moreover, it will be discussed how it could be improved in several ways.

2 INTEREST POINT DETECTORS

In this section both the Harris detector based on the structure tensor and the detector based on the determinant of the Hessian will be explained in detail. In the following section it will be shown how the spinor tensor is different but also very similar to the already explained techniques.

The image derivatives of an image I will be denoted I_x and I_y for the derivatives in the x and y direction respectively, and so on. These can be computed efficiently using convolution [Has14] and simple cubic filters were used for the presented evaluation.

2.1 The Structure Tensor

The Harris detector is based on the so called *structure tensor*, or second moment matrix, $\mathcal{T}$ of an image I, which is defined as

$$\mathcal{T} = \begin{bmatrix} I_x^2 & I_x I_y \\ I_x I_y & I_y^2 \end{bmatrix} \quad (1)$$

In the original paper, Harris and Stephens [HS88], proposed to compute the response using the trace and determinant of the matrix as

$$\mathcal{R} = det(\mathcal{T}) - k \cdot tr^2(\mathcal{T}), \quad (2)$$

where k is a constant, typically set to 0.04. However, the formulation by Noble [Nob89] will be

 ISBN 978-80-86943-71-8

used herein since it does not involve any constant and is therefore, in some sense more general. See also [Foe86]. The response is therefore computed as

$$\mathcal{R} = det(\mathcal{T})/(tr(\mathcal{T}) + \epsilon), \tag{3}$$

where ϵ is a small constant used to avoid division by zero. This approach will be referred to as *Harris* in the following sections. The geometrical interpretation of equation 2 is that it fires for corners, i.e. both eigenvalues λ_1 and λ_2 of the tensor $\mathcal{T}$ are high. Remember that

$$det(\mathcal{T}) = \lambda_1\lambda_2 \tag{4}$$
$$tr(\mathcal{T}) = \lambda_1 + \lambda_2 \tag{5}$$

Hence, the corners corresponds to where the response function $\mathcal{R}$ has its local maximas. Therefore, it is necessary to suppress non local maximas in the response [NVG06].

One of the key ideas is to make use of a Gaussian window, i.e. the elements in the matrix in equation 1 are filtered using a Gaussian kernel. This was an improvement compared to the early detector by Moravec [Mor80], which used a square window, yielding non isotropic responses. Nonetheless, the Gaussian is needed as the determinant would otherwise be zero. As an example, the determinant is computed as

$$det(\mathcal{T}) = (G(\sigma) * I_x^2)G(\sigma) * I_y^2 - (G(\sigma) * I_x I_y)^2 \tag{6}$$

The parameter σ will determine the size of the features being detected and a larger value will help detecting larger features. However, for clarity the Gaussian is omitted in the equations presented here.

2.2 Features by using the Hessian

The Hessian matrix used for SURF by Bay et al. [BETVG08], is defined as

$$\mathcal{H} = \begin{bmatrix} I_{xx} & I_{xy} \\ I_{xy} & I_{yy} \end{bmatrix} \tag{7}$$

They proposed to use the determinant of $\mathcal{H}$

$$det(\mathcal{H}) = I_{xx}I_{yy} - I_{xy}^2 \tag{8}$$

This approach will be referred to as *Hessian* in the subsequent sections. Furthermore, the trace can also be used for interest point detection and it can be noted that

$$tr(\mathcal{H}) = I_{xx} + I_{yy} = \nabla^2 I, \tag{9}$$

which is known as the Laplacian.

3 INTEREST POINTS FROM THE SPINOR TENSOR

Spinors form a subalgebra of geometric algebra [Hes71], which in its turn is a Clifford algebra. In fact quaternions are related to spinors.

Recently, the spinor tensor was derived by Batard and Berthier [BB13a] building on the work by Friedrich [Fri98]. It has got applications such as the spinor Fourier transform [BB13c, BB13b] and for color edge detection [BSJB09]. Especially, Berthier [Ber13] shows in details how to derive the spinor tensor from the fact there is an one to one correspondence between a spinor field φ^* of constant length on a Riemann surface and isometric immersions of the image, regarded as a 3D surface, where the gray level intensities are the height values of that surface.

The spinor tensor $\mathcal{S}_{\varphi^*}$, which is obtained from the derivative of the spinor field φ^* is defined as

$$\mathcal{S}_{\varphi^*} = \frac{1}{2(I_x^2 + I_y^2 + 1)^2} \begin{bmatrix} \mathcal{S}_{\varphi^*}^{11} & \mathcal{S}_{\varphi^*}^{12} \\ \mathcal{S}_{\varphi^*}^{21} & \mathcal{S}_{\varphi^*}^{22} \end{bmatrix} \tag{10}$$

with

$$\mathcal{S}_{\varphi^*}^{11} = I_{xx}^2 + I_{xy}^2 + I_{xx}^2 I_y^2 + I_{xy}^2 I_x^2 - 2I_{xx}I_{xy}I_xI_y \tag{11}$$
$$\mathcal{S}_{\varphi^*}^{22} = I_{yy}^2 + I_{xy}^2 + I_{yy}^2 I_x^2 + I_{xy}^2 I_y^2 - 2I_{yy}I_{xy}I_xI_y \tag{12}$$
$$\mathcal{S}_{\varphi^*}^{12} = I_{xx}I_{xy} + I_{xy}I_{yy} + I_{xx}I_{xy}I_y^2 + I_{xy}I_{yy}I_x^2 - I_{xy}^2 I_x I_y - I_{xx}I_{yy}I_xI_y \tag{13}$$
$$\mathcal{S}_{\varphi^*}^{21} = \mathcal{S}_{\varphi^*}^{12} \tag{14}$$

As already mentioned, a Gaussian window is typically applied to each of the elements of the matrices in equations 1 and 7 when the response is computed. In section 4 the response from doing this on equation 10 (with the factor multiplied into the matrix) is reported and it is obvious that both the determinant and the trace can be used as interest point detectors as well as the determinant divided by the trace as in equation 3. These approaches will be referred to as $Spinor_{det}$, $Spinor_{tr}$ and $Spinor_{det/tr}$, respectively in the subsequent sections.

Nonetheless, they will perform noticeably worse than the *Hessian* in equation 8. Therefore it was investigated what result could be obtained by using the expansions of both the determinant and the trace of equation 10 and then performing the Gaussian convolution on each of the resulting elements.

3.1 Simplifying the Determinant of the Spinor Tensor

The expansion and addition of the resulting 57 terms in the determinant of equation 10 is a simple but tedious algebraic exercise left for the reader and therefore only the final result is shown in the following equation

$$\begin{aligned} det(\mathcal{S}_{\varphi^*}) =& \frac{1}{2(I_x^2+I_y^2+1)^4} \\ & \big(I_{xy}^4 + I_x^2 I_{xy}^4 + I_y^2 I_{xy}^4 + I_{xx}^2 I_{yy}^2 \\ & -2I_y^2 I_{xx} I_{yy} I_{xy}^2 - 2I_x^2 I_{xx} I_{yy} I_{xy}^2 \\ & +I_x^2 I_{Ixx}^2 I_{yy}^2 + I_y^2 I_{xx}^2 I_{yy}^2 - 2I_{xx} I_{yy} I_{xy}^2\big) \end{aligned} \quad (15)$$

The right hand side of the expression can be factorized into

$$\frac{1}{2(I_x^2+I_y^2+1)^4}(I_{xx}I_{yy} - I_{xy}^2)^2(I_x^2+I_y^2+1) \quad (16)$$

The determinant of equation 10 can therefore be simplified as

$$det(\mathcal{S}_{\varphi^*}) = \frac{(I_{xx}I_{yy} - I_{xy}^2)^2}{2(I_x^2+I_y^2+1)^3} \quad (17)$$

Note that the dividend is actually the square of the determinant of the Hessian: $det^2(\mathcal{H})$. Furthermore, the divisor is related to the norm of the surface normal as explained by Batard and Berthier [BB13b]. Since the values of I_x^2 and I_y^2 are much smaller than 1, the divisor will have almost no impact on the final result as reported in section 4. Hence, the determinant of equation 10 and thereby the response can be computed as

$$\mathcal{R} = det^2(\mathcal{H}) \quad (18)$$

In fact, the result will be even better than for $Spinor_{det}$,as will also be shown in section 4, where this approach will be referred to as $Hessian^2$, which emphasizes what it in fact is.

The Geometrical interpretation of the Hessian matrix in equation 7 is that positive eigenvalues indicate a local maxima, negative ones indicate a local minima and different signs indicate a saddle point. Hence, the determinant in equation 8 will fire for local maximas only. Equation 18 will on the other hand fire for all these three cases since $(\lambda_1\lambda_2)^2$ will always be a positive value regardless of the type of point in question.

3.2 Simplifying the Trace

The trace of equation 10 can be factorized into

$$tr(\mathcal{S}_{\varphi^*}) = \frac{1}{2(I_x^2+I_y^2+1)^2} \quad (19)$$

$$\big((I_xI_{yy} - I_yI_{xy})^2 + (I_yI_{xx} - I_xI_{xy})^2 \quad (20)$$

$$+ I_{xx}^2 + I_{yy}^2 + 2I_{xy}^2\big) \quad (21)$$

Here it is important to note that the terms in equation 20 (after expansion) are all of higher degree than the terms of equation 21 and will therefore have almost no impact of the result, as will be shown in section 4. In fact 21 can be rewritten by removing the divisor, but keeping the constant, as

$$(1/2)\big(I_{xx}^2 + I_{yy}^2 + 2I_{xy}^2\big) = \quad (22)$$

$$(1/2)\big((I_{xx}+I_{yy})^2 - 2(I_{xx}I_{yy} - I_{xy}^2)\big) = \quad (23)$$

$$-\big((I_{xx}I_{yy} - I_{xy}^2) - (1/2)(I_{xx}+I_{yy})^2\big) \quad (24)$$

Note that the left term of equation 24 is the determinant of the Hessian and the right one is the trace of the same matrix. Also note that it is written in a form resembling equation 2, with $k = 1/2$. However, using the Hessian instead of the structure tensor. Hence the trace of the spinor tensor can be approximated by

$$\mathcal{R} = -\big(det(\mathcal{H}) - 1/2 \cdot tr^2(\mathcal{H})\big) \quad (25)$$

This approach will be referred to as *Harris of Hessian* from now on.

The geometrical interpretation of this response curve, still with the Hessian in mind, is the following

$$\begin{aligned} \mathcal{R} &= -\big(\lambda_1\lambda_2 - 1/2(\lambda_1+\lambda_2)^2\big) \\ &= \frac{\lambda_1^2+\lambda_2^2}{2} \end{aligned} \quad (26)$$

This implies that $\mathcal{R}$ will fire for all three mentioned cases as well. However, it will be enough that just one of the eigenvalues are large. Hence, it will detect edges rather than corners.

3.3 A new type of Interest Point Detector

It turns out that equation 20 can be used alone to compute the response as well. This time it is, however, not possible to rewrite the response as a determinant or the trace of a single tensor as it contains terms from both the structure tensor and the Hessian. Nevertheless, it is composed of two determinants

$$\mathcal{R} = det^2\begin{bmatrix} I_x & I_y \\ I_{xy} & I_{yy} \end{bmatrix} + det^2\begin{bmatrix} I_y & I_x \\ I_{xy} & I_{xx} \end{bmatrix} \quad (27)$$

This approach will be referred to as $Asymmetric^2$ from now on since it is based on the square of two asymmetric matrices.

 ISBN 978-80-86943-71-8

4 INVARIANCE TO ROTATION AND SCALE CHANGES

A series of testes were performed where the top 2500 feature points were computed for an image and also for a rotated variant of itself ($5° - 45°$ with step size $5°$) in order to find out whether if the detector is sensitive to rotations or not. The images were all cropped so that matching was performed on the inner circular disc, as shown in figure 1 and 2. The ratio between features appearing in the same position after rotation and the total number of features was computed. This was performed for triplets of images so that the mean result is computed. All distances less than 1.5 pixels in the original image was considered as being in the same position after rotation. Moreover, this was also done on an image downscaled to have sides that are 75% of their initial size, giving a scale of $1 : 4/3$.

Both figure 1 and 2 show three images to the left that were rotated and feature points extracted. The diagrams to the right show the average result from the three images, using both scale $1 : 1$ (upper bundle of curves) and $1 : 4/3$ (lower bundle of curves). The y-axis shows the ratio of feature points that are preserved during rotation and the x-axis shows σ. The $Hessian$ is depicted in blue and $Harris$ in green, in both diagrams, so that they could be easily compared with the spinor tensor and its variations. The diagram to the left shows $Spinor_{det}$ (red), $Spinor_{tr}$ (cyan) and $Spinor_{det/tr}$ (magenta). The diagram to the right shows $Hessian^2$ (red), $Asymmetric^2$ (equation 27) (cyan), $Harris\ of\ Hessian$ (equation 25) (magenta), $Hessian^2/Harris\ of\ Hessian$ (yellow). Where the latter is an approximation of $Spinor_{det/tr}$.

The σ was varied in the same way for the none rotated reference image and the rotated image. One can note that the upper three curves in each diagram come closer to a ratio of 1.0 than the lower ones do, since the upper represent the none scaled images.

In table 1 each triplet of images used in both figures was used to compute the similarity between pairs of detectors. In each column the percentage of detected points falling within a radius of 0.1 pixels is reported. The columns corresponds to A: $Hessian^2$, with our without the divisor. B: $Harris\ of\ Hessian$, one detector with both the divisor and the elements of equation 20, compared to the approach without both of them. C: $Hessian^2$ and $Harris\ of\ Hessian$ (both without divisor). D: $Hessian^2$ and $Asymmetric^2$. E: $Harris\ of\ Hessian$ (without divisor) and $Asymmetric^2$.

	A	B	C	D	E
1	99.81	99.57	5.87	0.03	0.39
2	99.88	99.74	7.89	0.00	0.27
3	99.63	99.34	10.07	0.00	0.73
1	99.87	99.61	5.08	0.02	10.27
2	99.47	96.27	2.17	0.00	0.18
3	99.74	99.39	2.82	0.01	0.28
4	99.83	99.53	5.20	0.08	0.55
5	99.66	99.37	7.54	0.00	0.28

Table 1: Comparison of how equal detectors are, showing the percentage of features detected within a radius of 0.1 pixels from each other of two different detectors. Each first three rows in the table corresponds to each row in figure 1, while the last four rows corresponds to each row in figure 2. A: $Hessian^2$ with and without divisor. B: $Harris\ of\ Hessian$ with divisor and elements of equation 20 or without both. C: $Hessian^2$ and $Harris\ of\ Hessian$ (both without divisor). D: $Hessian^2$ and $Asymmetric^2$. E: $Harris\ of\ Hessian$ and $Asymmetric^2$.

One can note (column A and B) that the divisor really is not necessary as it has a very small impact on the result, as already concluded. Moreover, the $Hessian^2$ and $Harris\ of\ Hessian$ (column C) are different but sometimes come close to each other. The $Asymmetric^2$ is, however, quite different from both of them.

5 DISCUSSION

It is very important that an interest point detector is invariant to rotation so that the response function will fire for the same positions (i.e. features) in the image, regardless of orientation. It is also desirable that the response function fires for the same features regardless of image scale. These are the reasons why one image was compared to a rotated variant of itself. Furthermore, the rotated image was down scaled in size, in a second evaluation, to investigate if the response function would still fire in the same places as for the original sized image. It can be noted that both $Hessian$ and $Harris$ do very well, almost regardless of σ for the first case, with rotation only. However, when there is a difference in scale it is obvious that σ will be more important. This is why the curves in the lower bundle has smaller peaks than the upper bundle of curves.

It was chosen to use three images for each diagram so that a mean value was computed for the ratio and it would be less dependent on that particular image. Moreover, it was considered de-

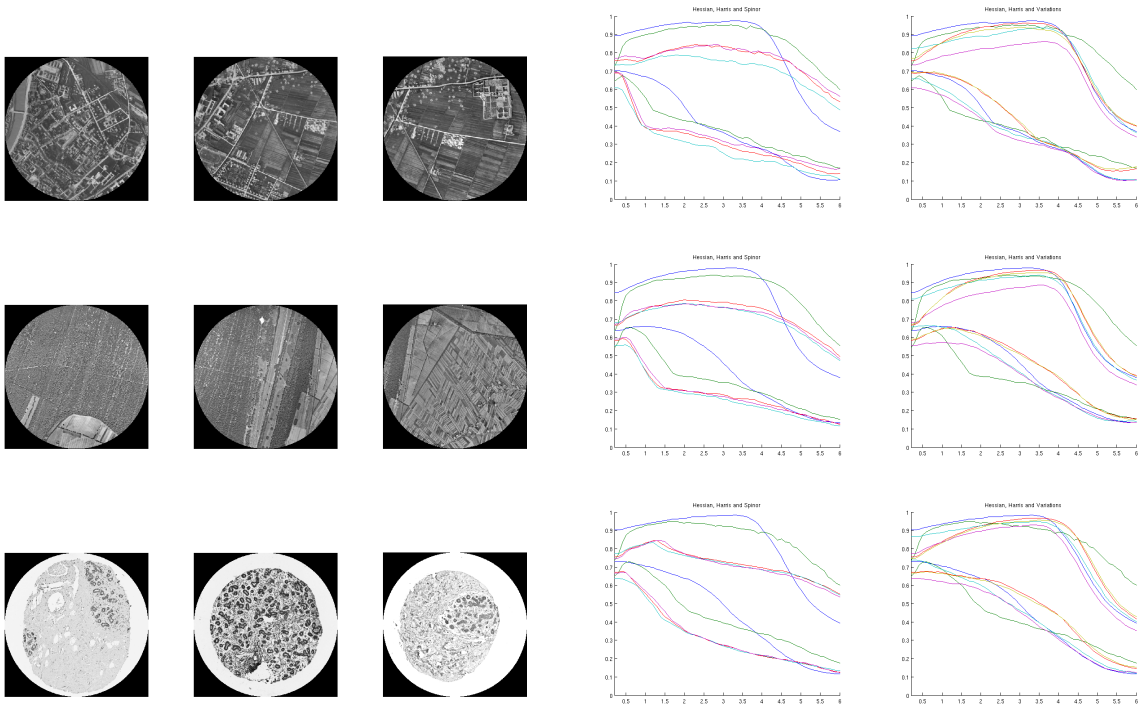

Figure 1: Evaluation of the invariance of the different detectors. The three images to the left were rotated and feature points extracted. The diagrams to the right show the average result from scale $1:1$ (upper curves) and $1:4/3$ (lower curves), where the y-axis shows the ratio of feature points that are preserved during rotation and the x-axis shows σ. The $Hessian$ is depicted in blue and $Harris$ in green, in both diagrams. The diagram to the left shows $Spinor_{det}$ (red), $Spinor_{tr}$ (cyan) and $Spinor_{det/tr}$ (magenta). The diagram to the right shows $Hessian^2$ (red), $Asymmetric^2$ (cyan), $Harris\ of\ Hessian$ (magenta) and $Hessian^2/Harris\ of\ Hessian$ (yellow). Two top rows ©MiBAC-ICCD, Aerofototeca Nazionale, fondo RAF. Third row ©The Human Protein Atlas (HPA) project [PSAE11].

sirable to test different groups of images showing different details. The first two rows in figure 1 contains historical aerial photos with two rather different characteristics. Row three shows breast tissue samples, while the rows in figure 2 show buildings and trees at different scales.

It was not investigated how the σ can be set by some kind of automatic scale space selection [Lin98, Lin99, MS01]. The proposed methods might benefit from using adaptive settings of σ and this is proposed for future research.

One can note several things from the diagrams in both figures. The diagrams to the left show that both $Hessian$ and $Harris$ generally performs better than $Spinor_{det}$, $Spinor_{tr}$ and $Spinor_{det/tr}$, with a few exceptions for certain values of σ.

The diagrams to the right, on the other hand, reveal that some of the so called variations, perform better and they are almost as good as the methods based on the structure tensor and the Hessian. In fact, they often do even better for images of different scales. One exception is the $Harris\ of\ Hessian$, which obviously has the worst performance, even if it for some images performs better than the three $Spinor$ approaches. The reason for this is most probably due to the fact that the response function in equation 26 will fire for situations where just one of the eigenvalues is large, i.e. edges are found rather than corners. It is clear from the diagrams that also $Spinor_{tr}$ generally performs worse than $Spinor_{det}$, since $Harris\ of\ Hessian$ is a valid approximation of $Spinor_{tr}$, i.e. it will also fire for edges.

One can also note that the $Hessian^2$ and $Hessian^2/Harris\ of\ Hessian$ performs almost equally good in all cases. The reason for this is that they often find the same interest points, or points close to one another, just as $Spinor_{det}$ and $Spinor_{det/tr}$ do. After all, the first two are variants of the latter. These facts are also visible in figure 3.

The $Asymmetric^2$ is perhaps the big surprise since it is just the residual of the trace of the spinor

 ISBN 978-80-86943-71-8

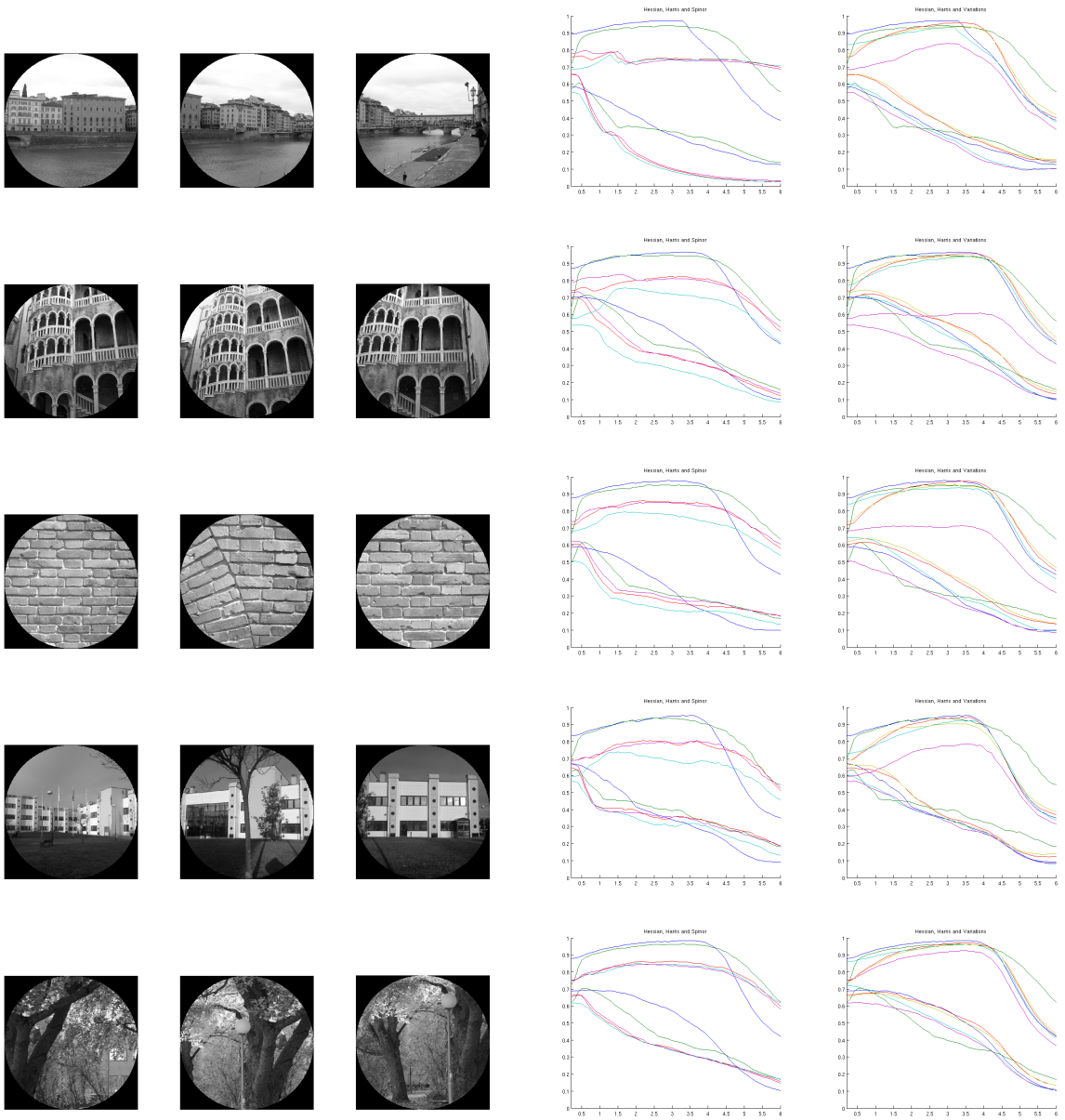

Figure 2: Evaluation of the invariance of the different detectors. The three images to the left were rotated and feature points extracted. The diagrams to the right show the average result from scale $1:1$ (upper curves) and $1:4/3$ (lower curves), where the y-axis shows the ratio of feature points that are preserved during rotation and the x-axis shows σ. The $Hessian$ is depicted in blue and $Harris$ in green, in both diagrams. The diagram to the left shows $Spinor_{det}$ (red), $Spinor_{tr}$ (cyan) and $Spinor_{det/tr}$ (magenta). The diagram to the right shows $Hessian^2$ (red), $Asymmetric^2$ (cyan), $Harris\ of\ Hessian$ (magenta) and $Hessian^2/Harris\ of\ Hessian$ (yellow). All images ©Anders Hast.

 ISBN 978-80-86943-71-8

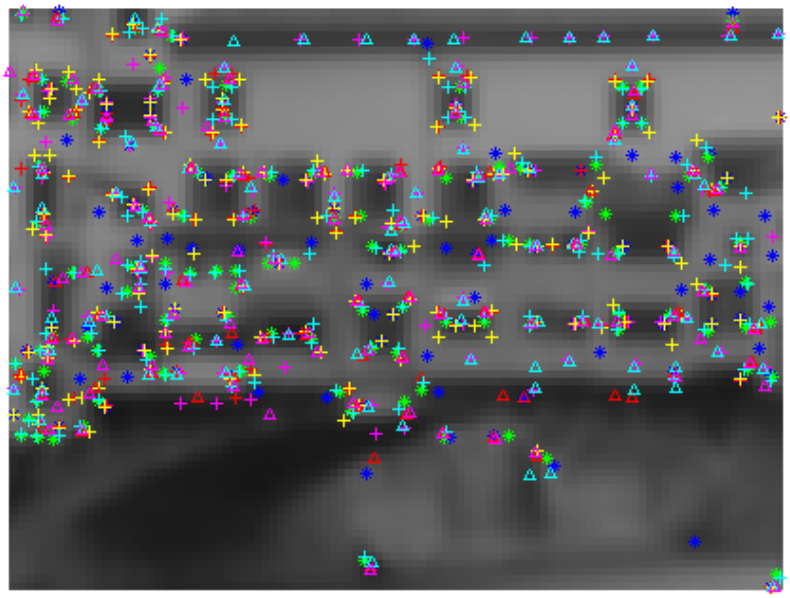

Figure 3: Comparison of different detectors, with a close-up of Ponte Vecchio in Florence (rightmost image, row 3 in figure 1) detected using $\sigma = 1.0$ with the following detectors: $Spinor_{det}$ (red Δ), $Spinor_{tr}$ (cyan Δ) and $Spinor_{det/tr}$ (magenta Δ), $Hessian^2$ (red $+$), $Asymmetric^2$ (cyan $+$), $Harris\ of\ Hessian$ (magenta $+$) and $Hessian^2/Harris\ of\ Hessian$ (yellow $+$).

tensor. Even if its impact on the trace is negligible, it still turns out to do very well when used as a response function on its own. For low values of σ it outperforms all other methods in most cases when scaling (lower bundle of curves). Actually it tend to follow the $Hessian$ even closer than what the $Hessian^2$ does.

One interesting question is: what is actually detected by the proposed detectors? In figure 3 an example is shown of the different detectors. It is obvious that some will find corners and others tend to be more sensitive to edges, like the long dark edge in the top of the image. To the latter category belongs $Spinor_{tr}$ and $harris\ of\ Hessian$. This is an direct effect of equation 26, which allow just one eigenvalue to be large.

Finally, it was concluded in the previous section that the divisors in equation 17 and 19 do almost have no impact at all for the images used in the tests as shown in table 1. Nevertheless, it should be kept in mind that the impact of the divisors will be larger for images with higher derivative variations. In any case, the detectors in question are proven to be invariant without the divisors.

6 CONCLUSION

Invariance with respect to rotation and scaling are two important features of any interest point detector. The determinant of the Hessian (DoH) and the Harris detectors are known to perform well for moderate changes in scale. The so called spinor tensor has recently been introduced and it was compared to these approaches. However, it turns out that they generally do noticeable worse. Therefore, some variations was introduced that do just as good or even better than both Harris and DoH, especially for differences in scale. These variations are based on expansions of the determinant and the trace and many terms will cancel out, giving at hand simpler formulations.

7 FUTURE WORK

The proposed variations of the spinor tensor's determinant and trace should be investigated further. Especially it is interesting to find out what automatic scale space selection would add to their performance when it comes to scale differences.

Moreover, it seems likely that the approach referred to as $Asymmetric^2$ could be described in another way than presented here, i.e. as the sum of the square of two asymmetric determinants. Perhaps there are some symmetric tensor that describes the very same thing, still waiting to be found.

8 ACKNOWLEDGEMENT

The features was obtained using a sub pixel accuracy method, found in `nonmaxsuppts.m`, by [Kov14].

9 REFERENCES

[BB13a] Batard T., Berthier M.: Clifford-fourier transform and spinor representation of images. In *Quaternion and Clifford Fourier Transforms and Wavelets*, Hitzer E., Sangwine S. J., (Eds.), Trends in Mathematics. Springer Basel, 2013, pp. 177–195.

[BB13b] Batard T., Berthier M.: A riemannian fourier transform via spin representations. In *GSI* (2013), Nielsen F., Barbaresco F., (Eds.), vol. 8085 of *Lecture Notes in Computer Science*, Springer, pp. 131–139.

[BB13c] Batard T., Berthier M.: Spinor fourier transform for image processing. *J. Sel. Topics Signal Processing 7*, 4 (2013), 605–613.

[Ber13] Berthier M.: Spin geometry and image processing. *Advances in Applied Clifford Algebras* (2013), 1–20.

[BETVG08] Bay H., Ess A., Tuytelaars T., Van Gool L.: Speeded-up robust features (surf). *Comput. Vis. Image Underst. 110*, 3 (June 2008), 346–359.

[BL07] Brown M., Lowe D. G.: Automatic panoramic image stitching using invariant features. *International Journal of Computer Vision 74*, 1 (2007), 59–73.

[BSJB09] Batard T., Saint-Jean C., Berthier M.: A metric approach to nd images edge detection with clifford algebras. *Journal of Mathematical Imaging and Vision 33*, 3 (2009), 296–312.

[Foe86] Foerstner W.: A Feature Based Correspondence Algorithm for Image Matching. *Int. Arch. of Photogrammetry and Remote Sensing 26*, 3 (1986), 150–166.

[Fri98] Friedrich T.: On the spinor representation of surfaces in Euclidean 3-space. *J. Geom. Phys. 28*, 1-2 (1998), 143–157.

[GHT11] Gauglitz S., Höllerer T., Turk M.: Evaluation of interest point detectors and feature descriptors for visual tracking. *Int. J. Comput. Vision 94*, 3 (Sept. 2011), 335–360.

[Has14] Hast A.: Simple filter design for first and second order derivatives by a double filtering approach. *Pattern Recognition Letters 42*, 0 (2014), 65 – 71.

[Hes71] Hestenes D.: Vectors, Spinors, and Complex Numbers in Classical and Quantum Physics. *American Journal of Physics 39*, 9 (Sept. 1971), 1013–1027.

[HS88] Harris C., Stephens M.: A combined corner and edge detection. In *Alvey Vision Conference* (1988), pp. 147–151.

[Kov14] Kovesi P.: Matlab and octave functions for computer vision and image processing, 2014.

[Lin98] Lindeberg T.: Feature detection with automatic scale selection. *Int. J. Comput. Vision 30*, 2 (Nov. 1998), 79–116.

[Lin99] Lindeberg T.: Principles for automatic scale selection. *Handbook on computer vision and applications 2* (1999), 239–274.

[Low04] Lowe D. G.: Distinctive image features from scale-invariant keypoints. *International Journal of Computer Vision 60*, 2 (2004), 91–110.

[Mor80] Moravec H. P.: *Obstacle avoidance and navigation in the real world by a seeing robot rover*. PhD thesis, Stanford University, Stanford, CA, USA, 1980. AAI8024717.

[MS01] Mikolajczyk K., Schmid C.: Indexing based on scale invariant interest points. In *In Proceedings of the 8th International Conference on Computer Vision* (2001), pp. 525–531.

[Nob89] Noble J. A.: *Descriptions of image surfaces*. PhD thesis, Oxford University, St Hugh's College, Oxford, GB, 1989. Ph. D. : Engineering sci. : April.

[NVG06] Neubeck A., Van Gool L.: Efficient non-maximum suppression. In *Proceedings of the 18th International Conference on Pattern Recognition - Volume 03* (Washington, DC, USA, 2006), ICPR '06, IEEE Computer Society, pp. 850–855.

[PSAE11] Ponten F., Schwenk J. M., Asplund A., Edqvist P. H.: The human protein atlas as a proteomic resource for biomarker discovery. *Journal of Internal Medicine 270*, 5 (2011), 428–446. QC 20111212.

[SB97] Smith S. M., Brady J. M.: Susan - a new approach to low level image processing. *Int. J. Comput. Vision 23*, 1 (May 1997), 45–78.

[SMB98] Schmid C., Mohr R., Bauckhage C.: Comparing and Evaluating Interest Points. In *6th International Conference on Computer Vision (ICCV '98)* (Bombay, Inde, 1998), IEEE Computer society, pp. 230–235.

[SMB00] Schmid C., Mohr R., Bauckhage C.: Evaluation of interest point detectors. *Int. J. Comput. Vision 37*, 2 (June 2000), 151–172.

[ST94] Shi J., Tomasi C.: Good features to track. In *Computer Vision and Pattern Recognition, 1994. Proceedings CVPR '94., 1994 IEEE Computer Society Conference on* (June 1994), IEEE, pp. 593–600.

[Sze06] Szeliski R.: Image alignment and stitching: a tutorial. *Found. Trends. Comput. Graph. Vis. 2*, 1 (January 2006), 1–104.

[TH98] Trajkovic M., Hedley M.: Fast corner detection. *Image and Vision Computing 16*, 2 (1998), 75 – 87.

[TM07] Tuytelaars T., Mikolajczyk K.: Local invariant feature detectors: A survey. *Foundations and Trends¨ in Computer Graphics and Vision 3*, 3 (2007), 177–280.

[ZKM04] Zuliani M., Kenney C., Manjunath B. S.: A mathematical comparison of point detectors. In *Second IEEE Image and Video Registration Workshop (IVR)* (Jun 2004), pp. 172–178.